Journal of Nonlinear Modeling and Analysis
Volume 7, Number 5, October 2025, 1940–1964
https://journal.global-sci.org/jnma
DOI:10.12150/jnma.2025.1940

A Multiscale Coupled Reaction-Diffusion Model of Amyloid-Beta and Tau Pathology in Alzheimer's Disease

Aytekin Enver[1,†], Fatma Ayaz[2] and Deniz Eylem Yalçınkaya[3]

Abstract Alzheimer's disease (AD) is a progressive neurodegenerative disorder characterized by the accumulation of amyloid-beta (Aβ) plaques and tau neurofibrillary tangles (NFTs), as well as by chronic neuroinflammation and blood-brain barrier (BBB) dysfunction. Although these pathological features are well known, their complex interactions remain poorly understood. This study proposes a comprehensive multiscale coupled reaction-diffusion model composed of 13 partial differential equations to simulate the spatio-temporal dynamics of Aβ and tau pathology, neuroinflammatory responses, BBB integrity, and neuronal degeneration. The model captures biochemical reaction kinetics, diffusion-driven propagation, and regulatory feedback among key cellular components, including microglia, astrocytes, and cytokines. Furthermore, the effects of therapeutic interventions, such as anti-amyloid drugs and dietary modifications, are incorporated to assess their influence on disease progression. Numerical simulations using finite difference methods provide insights into how these factors contribute to or mitigate AD pathogenesis. The results support the potential of mathematical modeling as a tool to understand disease mechanisms and evaluate treatment strategies.

Keywords Alzheimer's disease, amyloid-beta, tau pathology, reaction-diffusion models, neurodegeneration, mathematical modeling

MSC(2010) 34K28, 93A30, 35Q92.

1. Introduction

Alzheimer's disease (AD) is the most prevalent progressive neurodegenerative disorder characterized by cognitive impairment, neuronal degeneration, and synaptic failure. Alzheimer's disease (AD) pathogenic hallmarks consist primarily of extracellular deposition of amyloid-beta (Aβ) plaques and intracellular accumulation of tau neurofibrillary tangles (NFTs), resulting in diffuse neuronal damage and synaptic loss [1–4]. Despite decades of research, AD remains an incurable disease even today, which emphasizes the importance of mathematical modeling as an instrumental asset towards understanding disease progression and evaluating pharmacologic

[†]The corresponding author.
Email address: aytekinanwer@gmail.com (Aytekin Enver), fayaz@gazi.edu.tr (Fatma Ayaz), deylem76@yahoo.com (Deniz Eylem Yalçınkaya)
[1]Graduate School of Natural and Applied Sciences, Department of Mathematics, Gazi University, Besevler, 06550, Türkiye
[2]Department of Mathematics, Gazi University, Besevler, 06550, Türkiye
[3]Department of Neurology, Ankara Private Koru Hospital, Kavaklidere, 06550, Türkiye

intervention capable of delaying disease progression [5–8].

2. History and development of mathematical modeling in Alzheimer's disease

Alzheimer's disease (AD) is a progressive neurodegenerative disorder first described by Alois Alzheimer in 1906 [9–12]. Characteristic features of AD pathology include amyloid-beta (Aβ) plaques, tau neurofibrillary tangles (NFTs), neuronal death, and synaptic dysfunction. Although clinical and biological research has improved in elucidating the disease, mathematical modeling has been critical in offering a quantitative and predictive foundation for the study of the disease's evolution and potential treatment approaches [13].

2.1. Early theoretical approaches (1970s–1990s)

Mathematical models in neuroscience were dominated by neuronal networks and electrophysiology in the early years (Hodgkin & Huxley, 1952) [14]. However, at least as early as the 1980s and 1990s, researchers began developing compartmental models of neurodegeneration processes.

Linear Compartmental Models: Previous models of AD employed compartmental kinetics to depict amyloid-beta production, clearance, and aggregation [15]. Despite their simplicity, these models were critical for measuring the protein turnover rates occurring in the brain [16, 17].

Population-Based Models: Such epidemiological models were built to understand the incidence and progression of AD across diverse populations. Using these models helped estimate risk factors of disease and effectiveness of public health interventions [18].

2.2. Expansion into biochemical and cellular models (2000s–2020s)

With advances in molecular biology and imaging, mathematical models became more mechanistic, incorporating biochemical pathways of protein aggregation and neuronal damage.

Reaction-Kinetics Models (2000s): These models described Aβ and tau aggregation using reaction-diffusion equations, modeling how monomers transition into oligomers and fibrils [19–21].

Neuronal Network-Based Models: Computational neuroscience methods used graph theory to characterize the loss of connectivity in neuronal networks, modeling how synaptic damage spreads in time [22].

Inflammation and Immune Response Models: Researchers incorporated the role of microglia and cytokines, demonstrating how neuroinflammation contributes to AD pathology [23].

2.3. Modern reaction-diffusion and multi-scale models

Recent research has mostly focused on spatially explicit reaction-diffusion models, which also aim to simulate the spread of pathology (both amyloid-beta and tau)

through various brain regions [4, 6, 24, 25].

Turing Pattern Formation in AD: Researchers explored diffusion-driven instabilities (Turing patterns) in amyloid-beta and tau propagation, revealing spatial heterogeneities in plaque formation [26].

Coupled Reaction-Diffusion Models for Multi-Pathway Interactions (2020s): Current models integrate biochemical, immunological, and vascular interactions, including:

- Amyloid-beta and tau kinetics.
- Neuroinflammation (cytokine-mediated interactions).
- Blood-brain barrier integrity.
- Effects of drugs and dietary interventions.

2.4. Advancements and insights on Alzheimer's disease after 2020

In the last few years, the mathematical modeling of Alzheimer's disease (AD) has progressed rapidly, using sophisticated methods to elucidate pathophysiology and disease trajectory. Challenged in their underlying simplicity, these contemporary models aspire to incorporate many biological, genetic and clinical data to create a more comprehensive picture of AD.

1. Biomarker Dynamics and Disease Progression Models: Recently researchers have developed a series of mathematical models that encapsulate the temporal progression of AD-related biological markers and cognitive decline. For example, a multidimensional ordinary differential equation (ODE)-based model was presented to describe different trajectories in biomarker space as a function of time since diagnosis and to make personalized predictions about disease progression [27]. Another study focused on a mathematical representation of the AD biomarker cascade, specifically citing statistical difficulties in the identification of neurobiological disease surrogates [28–31].

2. Multiscale and Multidimensional Modeling Approaches: Advances have been made in the development of multiscale models that encompass all levels of biology from molecular interactions to system-wide effects. A computational model of the progression of AD via a 19 ODE system was presented to represent the interactions in AD pathology across nano, micro, and macro levels [30]. Furthermore, researchers elaborated the interaction of amyloid-beta and calcium levels based on a data-driven stochastic model, helping quantify their effects on AD progression [32, 33].

3. Modeling the Impact of Therapeutics: Models have also been used to simulate therapeutic agents on AD biomarkers. These studies illustrated the utility of mathematical frameworks in predicting the response of the disease to different inhibitors during the course of the illness, informing the assessment of potentially promising therapeutic interventions. The authors emphasized the collaborative and transformative nature of the mathematical modeling methodology in AD-related research, which remains a key strategy to navigate the complex pathogenesis of AD and to formulate possible treatment strategies [34, 35].

3. Mathematical modeling for Alzheimer disease

Mathematical modeling offers insights into complex biological systems, including the processes that give rise to neurodegenerative diseases like Alzheimer's. Biological processes can be represented with mathematical equations, making it possible to identify patterns and predict how these systems will behave under various conditions. This is particularly the case for reaction-diffusion equations which are fundamental for modeling the spatiotemporal dynamics of biological molecules, cells, and tissues. These equations describe spatial- and temporal-regulated dynamics of substances (e.g., proteins, cytokines) as they diffuse in space and interact with each other in time [24, 36, 37].

In the context of Alzheimer's disease, researchers have characterized the dynamics of amyloid-beta (Aβ) and tau proteins, microglia, astrocytes, cytokines, integrity of the blood-brain barrier, and neuronal density, described by a system of 13 equations. Further sections explain what each variable means in each equation and its significance [38, 39].

3.1. Amyloid-beta monomers (A_m)

$$\frac{\partial A_m}{\partial t} = D_{A_m}\nabla^2 A_m + P_{A_m}(x) + \left(k_{n,A}A_m + k_{s,TA}^{(mo)}A_m T_o\right) - k_{c,m}A_m h_{BBB}(B(x,t)) - \Phi_m(C)A_m - \gamma_{drug,A_m}A_m - \gamma_{diet,A_m}A_m, \tag{3.1}$$

where A_m is the concentration of amyloid-beta monomers, D_{A_m} is the diffusion coefficient of amyloid-beta monomers, $P_{A_m}(x)$ is the production rate of amyloid-beta monomers, $k_{n,A}$ is the rate constant for nucleation into oligomers, $k_{s,TA}^{(mo)}$ is the rate constant for secondary nucleation in presence of tau oligomers, $k_{c,m}$ is the clearance rate of amyloid-beta monomers, $h_{BBB}(B(x,t))$ represents the effect of blood-brain barrier integrity on clearance, $\Phi_m(C)$ represents the effect of cytokines on degradation, γ_{drug,A_m} is the effect of drugs on amyloid-beta monomers, and γ_{diet,A_m} is the effect of diet on amyloid-beta monomers.

3.2. Amyloid-beta oligomers (A_o)

$$\frac{\partial A_o}{\partial t} = D_{A_o}\nabla^2 A_o + \left(k_{n,A}A_m + k_{s,TA}^{(mo)}A_m T_o\right) + k_{frag,A}A_f - \left(k_{f,A}A_o + k_{s,TA}^{(of)}A_o T_f\right) - k_{c,o}(A_o; M_{pro}, M_{Anti}, A_{s1}, A_{s2}) - \Phi_o(C)A_o - \gamma_{drug,A_o}A_o - \gamma_{diet,A_o}A_o, \tag{3.2}$$

where A_o is the concentration of amyloid-beta oligomers, D_{A_o} is the diffusion coefficient of amyloid-beta oligomers, $k_{n,A}$ is the rate constant for nucleation of A_m, $k_{s,TA}^{(mo)}$ is the rate constant for secondary nucleation in presence of tau oligomers, $k_{frag,A}$ is the rate constant for fragmentation of amyloid-beta fibrils into oligomers, $k_{f,A}$ is the rate constant for fibrillization of A_o, $k_{s,TA}^{(of)}$ is the rate constant for secondary nucleation with tau fibrils, $k_{c,o}(A_o; M_{pro}, M_{Anti}, A_{s1}, A_{s2})$ is the clearance rate of A_o depending on microglia and astrocytes, $\Phi_o(C)$ is the effect of cytokines

on A_o degradation, γ_{drug,A_o} is the effect of drugs on A_o, and γ_{diet,A_o} is the effect of diet on A_o.

3.3. Amyloid-beta fibrils (A_f)

$$\frac{\partial A_f}{\partial t} = D_{A_f}\nabla^2 A_f + \left(k_{f,A}A_o + k_{s,TA}^{(of)}A_f T_f\right) - k_{frag,A}A_f - k_{c,f}(A_f; M_{pro}, M_{Anti}, A_{s1}, A_{s2}) - \Phi_f(C)A_f - \gamma_{drug,A_f}A_f - \gamma_{diet,A_f}A_f, \tag{3.3}$$

where A_f is the concentration of amyloid-beta fibrils, D_{A_f} is the diffusion coefficient of amyloid-beta fibrils, $k_{f,A}$ is the rate constant for fibrillization of A_o, $k_{s,TA}^{(of)}$ is the rate constant for secondary nucleation in the presence of tau fibrils, $k_{frag,A}$ is the rate constant for fragmentation of A_f into oligomers, $k_{c,f}(A_f; M_{pro}, M_{Anti}, A_{s1}, A_{s2})$ is the clearance rate of A_f depending on microglia and astrocytes, $\Phi_f(C)$ is the effect of cytokines on A_f degradation, γ_{drug,A_f} is the effect of drugs on A_f, and γ_{diet,A_f} is the effect of diet on A_f.

3.4. Tau monomers (T_m)

$$\frac{\partial T_m}{\partial t} = D_{T_m}\nabla^2 T_m + P_{T_m}(x) - \left(k_{n,T}T_m + k_{s,AT}^{(mo)}T_m A_o\right) - k_{c,m}^{(T)}T_m h_{BBB}(B(x,t)) - \Phi_m^T(C)T_m - \gamma_{drug,T_m}T_m - \gamma_{diet,T_m}T_m, \tag{3.4}$$

where T_m is the concentration of tau monomers, D_{T_m} is the diffusion coefficient of tau monomers, $P_{T_m}(x)$ is the production rate of tau monomers, $k_{n,T}$ is the rate constant for nucleation of T_m into oligomers, $k_{s,AT}^{(mo)}$ is the rate constant for secondary nucleation of T_m in presence of amyloid-beta oligomers, $k_{c,m}^{(T)}$ is the clearance rate of tau monomers affected by BBB, $h_{BBB}(B(x,t))$ represents blood-brain barrier integrity, $\Phi_m^T(C)$ is the effect of cytokines on T_m degradation, γ_{drug,T_m} is the effect of drugs on T_m, and γ_{diet,T_m} is the effect of diet on T_m.

3.5. Tau oligomers (T_o)

$$\frac{\partial T_o}{\partial t} = D_{T_o}\nabla^2 T_o + \left(k_{n,T}T_m + k_{s,AT}^{(mo)}T_m A_o\right) - k_{frag,T}T_f - \left(k_{f,T}T_o + k_{s,AT}^{(of)}T_o A_f\right) - k_{c,o}^{(T)}(T_o; M_{pro}, M_{Anti}, A_{s1}, A_{s2}) - \Phi_o^T(C)T_o - \gamma_{drug,T_o}T_o - \gamma_{diet,T_o}T_o, \tag{3.5}$$

where T_o is the concentration of tau oligomers, D_{T_o} is the diffusion coefficient of tau oligomers, $k_{n,T}$ is the nucleation rate of T_m, $k_{s,AT}^{(mo)}$ is the secondary nucleation rate of T_m in presence of A_o, $k_{frag,T}$ is the fragmentation rate of tau fibrils into oligomers, $k_{f,T}$ is the fibrillization rate of T_o, $k_{s,AT}^{(of)}$ is the secondary nucleation rate of T_o in presence of A_f, $k_{c,o}^{(T)}(T_o; M_{pro}, M_{Anti}, A_{s1}, A_{s2})$ is the clearance rate of T_o dependent on microglia and astrocytes, $\Phi_o^T(C)$ is the effect of cytokines on T_o degradation, γ_{drug,T_o} is the effect of drugs on T_o, and γ_{diet,T_o} is the effect of diet on T_o.

3.6. Tau fibrils (T_f)

$$\frac{\partial T_f}{\partial t} = D_{T_f}\nabla^2 T_f + \left(k_{f,T}T_o + k_{s,AT}^{(of)}T_o A_f\right) - k_{frag,T}T_f - k_{c,f}^{(T)}(T_f; M_{pro}, M_{Anti}, A_{s1}, A_{s2}) - \Phi_f^T(C)T_f - \gamma_{drug,T_f}T_f - \gamma_{diet,T_f}T_f, \tag{3.6}$$

where T_f is the concentration of tau fibrils, D_{T_f} is the diffusion coefficient of tau fibrils, $k_{f,T}$ is the fibrillization rate of T_o, $k_{s,AT}^{(of)}$ is the secondary nucleation rate of T_o in the presence of A_f, $k_{frag,T}$ is the fragmentation rate of T_f into oligomers, $k_{c,f}^{(T)}(T_f; M_{pro}, M_{Anti}, A_{s1}, A_{s2})$ is the clearance rate of T_f dependent on microglia and astrocytes, $\Phi_f^T(C)$ is the effect of cytokines on T_f degradation, γ_{drug,T_f} is the effect of drugs on T_f, and γ_{diet,T_f} is the effect of diet on T_f.

3.7. Pro-inflammatory microglia ($M_{\mathbf{pro}}$)

$$\frac{\partial M_{\text{pro}}}{\partial t} = D_M\nabla^2 M_{\text{pro}} + \alpha_1(A_o + T_o)M_{\text{anti}} - \alpha_2 M_{\text{pro}} - \beta_{M_{\text{pro}}}M_{\text{pro}} - \gamma_{drug,M_{\text{pro}}}M_{\text{pro}} - \gamma_{diet,M_{\text{pro}}}M_{\text{pro}}, \tag{3.7}$$

where M_{pro} is the concentration of pro-inflammatory microglia, D_M is the diffusion coefficient of microglia, α_1 is the activation rate of pro-inflammatory microglia by A_o and T_o, α_2 is the deactivation rate of pro-inflammatory microglia, $\beta_{M_{\text{pro}}}$ is the natural decay rate of M_{pro}, $\gamma_{drug,M_{\text{pro}}}$ is the effect of drugs on M_{pro}, and $\gamma_{diet,M_{\text{pro}}}$ is the effect of diet on M_{pro}.

3.8. Anti-inflammatory microglia ($M_{\mathbf{anti}}$)

$$\frac{\partial M_{\text{anti}}}{\partial t} = D_M\nabla^2 M_{\text{anti}} + \alpha_2 M_{\text{pro}} - \alpha_1(A_o + T_o)M_{\text{anti}} - \beta_{M_{\text{anti}}}M_{\text{anti}} + \gamma_{drug,M_{\text{anti}}}M_{\text{anti}} + \gamma_{diet,M_{\text{anti}}}M_{\text{anti}}, \tag{3.8}$$

where M_{anti} is the concentration of anti-inflammatory microglia, D_M is the diffusion coefficient of microglia, α_2 is the conversion rate from pro-inflammatory to anti-inflammatory state, α_1 is the reactivation rate by amyloid-beta and tau oligomers, $\beta_{M_{\text{anti}}}$ is the natural decay rate of M_{anti}, $\gamma_{drug,M_{\text{anti}}}$ is the effect of drugs on M_{anti}, and $\gamma_{diet,M_{\text{anti}}}$ is the effect of diet on M_{anti}.

3.9. Harmful astrocytes (A_{s1})

$$\frac{\partial A_{s1}}{\partial t} = D_{A_s}\nabla^2 A_{s1} + \gamma_1(A_o + T_o)A_{s2} - \gamma_2 A_{s1} - \beta_{A_{s1}}A_{s1} - \gamma_{drug,A_{s1}}A_{s1} - \gamma_{diet,A_{s1}}A_{s1}, \tag{3.9}$$

where A_{s1} is the concentration of harmful astrocytes, D_{A_s} is the diffusion coefficient of astrocytes, γ_1 is the activation rate of A_{s1} by A_o and T_o, γ_2 is the deactivation rate of A_{s1}, $\beta_{A_{s1}}$ is the natural decay rate of A_{s1}, $\gamma_{drug,A_{s1}}$ is the effect of drugs on A_{s1}, and $\gamma_{diet,A_{s1}}$ is the effect of diet on A_{s1}.

3.10. Protective astrocytes (A_{s2})

$$\frac{\partial A_{s2}}{\partial t} = D_{A_s}\nabla^2 A_{s2} + \gamma_2 A_{s1} - \gamma_1(A_o + T_o)A_{s2} - \beta_{A_{s2}}A_{s2} + \gamma_{drug,A_{s2}}A_{s2} + \gamma_{diet,A_{s2}}A_{s2}, \tag{3.10}$$

where A_{s2} is the concentration of protective astrocytes, D_{A_s} is the diffusion coefficient of astrocytes, γ_2 is the conversion rate from A_{s1} to A_{s2}, γ_1 is the rate of reactivation into harmful astrocytes by A_o and T_o, $\beta_{A_{s2}}$ is the natural decay rate of A_{s2}, $\gamma_{drug,A_{s2}}$ is the effect of drugs on A_{s2}, and $\gamma_{diet,A_{s2}}$ is the effect of diet on A_{s2}.

3.11. Cytokines (C)

$$\frac{\partial C}{\partial t} = D_C\nabla^2 C + \eta_{M_{\text{pro}}}M_{\text{pro}} + \eta_{A_{s1}} - k_C C - \gamma_{drug,C}C - \eta_{diet,C}C, \tag{3.11}$$

where C is the concentration of cytokines, D_C is the diffusion coefficient of cytokines, $\eta_{M_{\text{pro}}}$ is the production rate of cytokines by pro-inflammatory microglia, $\eta_{A_{s1}}$ is the production rate of cytokines by harmful astrocytes, k_C is the degradation rate of cytokines, $\gamma_{drug,C}$ is the effect of drugs on cytokines, and $\eta_{diet,C}$ is the effect of diet on cytokines.

3.12. Blood-brain barrier integrity (B)

$$\frac{\partial B}{\partial t} = D_B\nabla^2 B - k_{\text{deg},B}(A_o + T_o + C)B + r_{\text{rec}}(1 - B) + \gamma_{drug,B}B + \eta_{diet,B}B, \tag{3.12}$$

where B is the integrity of the blood-brain barrier, D_B is the diffusion coefficient of blood-brain barrier components, $k_{\text{deg},B}$ is the degradation rate of B due to A_o, T_o, and C, r_{rec} is the recovery rate of the blood-brain barrier, and $\gamma_{drug,B}$ is the effect of drugs on B, $\eta_{diet,B}$ is the effect of diet on B.

3.13. Neuronal density (N)

$$\frac{\partial N}{\partial t} = D_N\nabla^2 N - \mu_N(A_o + T_o)N + \lambda_{\text{growth}}(N_{\max} - N) - \phi_N(C)N + \gamma_{drug,N}N + \eta_{diet,N}N, \tag{3.13}$$

where N is the neuronal density, D_N is the diffusion coefficient of neurons, μ_N is the neuronal death rate due to A_o and T_o, λ_{growth} is the neuronal growth rate, $N_{\max}$ is the maximum neuronal density, $\phi_N(C)$ is the effect of cytokines on neuronal death, and $\gamma_{drug,N}$ is the effect of drugs on N, $\eta_{diet,N}$ is the effect of diet on N.

3.14. Parameters for amyloid-beta, tau, microglia, cytokines, blood-brain barrier, and neuronal dynamics in Alzheimer's disease

Table 1. Parameters for Amyloid-Beta Monomer Dynamics

Parameter	Description	Example Value	Units	Source
D_{A_m}	Diffusion coefficient of amyloid-beta monomers	0.1	mm^2/day	[37]
$P_{A_m}(x)$	Production rate of amyloid-beta monomers at position x	0.05	μM/day	[40]
$k_{n,A}$	Natural degradation rate of amyloid-beta monomers	0.05	1/day	[37]
$k_{s,TA}^{(m)}$	Interaction rate between amyloid-beta monomers and tau oligomers	0.01	1/(day·μM)	[37]
$k_{c,m}$	Clearance rate of amyloid-beta monomers via the blood-brain barrier	0.02	1/(day·μM)	[41]
$h_{\text{BBB}}(B(x,t))$	Blood-brain barrier integrity function (spatial and temporal dependence)	0.1	1/day	Specific studies required
$\Phi_m(C)$	Microglial phagocytosis rate of amyloid-beta monomers influenced by cytokine levels	0.03	1/day	[37]
γ_{drug,A_m}	Aducanumab-induced degradation rate of amyloid-beta monomers	0.04–0.06	1/day	[41]

Table 2. Parameters for Amyloid-Beta Oligomer Dynamics

Parameter	Description	Example Value	Units	Source
η_{diet,A_m}	Mediterranean diet-induced modulation rate of amyloid-beta monomers	0.03–0.05	1/day	[40]
D_{A_o}	Diffusion coefficient of amyloid-beta oligomers	0.05	mm^2/day	[37]
$k_{s,TA}^{(mo)}$	Interaction rate between amyloid-beta monomers and tau oligomers	0.01	1/(day·μM)	[37]
$k_{\text{frag},A}$	Fragmentation rate of amyloid-beta fibrils	0.01	1/day	[37]
$k_{f,A}$	Fibrillization rate of amyloid-beta oligomers	0.02	1/day	[37]
$k_{s,TA}^{(of)}$	Interaction rate between amyloid-beta oligomers and tau fibrils	0.02	1/(day·μM)	Specific studies required
$k_{c,o}$	Clearance rate of amyloid-beta oligomers by microglia and other immune cells	0.015	1/(day·μM)	[37]
$\Phi_o(C)$	Cytokine-dependent microglial clearance rate of amyloid-beta oligomers	0.02–0.03	1/day	[41]

Table 3. Parameters for Amyloid-Beta Fibrils and Tau Monomers

Parameter	Description	Example Value	Units	Source
γ_{drug,A_o}	Solanezumab-induced clearance rate of amyloid-beta oligomers	0.03–0.05	1/day	[42]
η_{diet,A_o}	Anti-inflammatory diet-induced modulation rate of amyloid-beta oligomers	0.02–0.04	1/day	[43]
D_{A_f}	Diffusion coefficient of amyloid-beta fibrils	0.01–0.05	mm^2/day	[37]
$k_{c,f}$	Clearance rate of amyloid-beta fibrils by microglia and astrocytes	0.015–0.02	1/(day·μM)	Specific studies required
$\Phi_f(C)$	Cytokine-dependent microglial clearance rate of amyloid-beta fibrils	0.02	1/day	[41]
γ_{drug,A_f}	Aducanumab-induced clearance rate of amyloid-beta fibrils	0.02–0.04	1/day	[44]
η_{diet,A_f}	Ketogenic diet-induced clearance rate of amyloid-beta fibrils	0.015–0.03	1/day	[45]
D_{T_m}	Diffusion coefficient of tau monomers	0.05–0.1	mm^2/day	[46]

Table 4. Parameters for Tau Monomers and Tau Oligomers

Parameter	Description	Example Value	Units	Source
$P_{T_m}(x)$	Production rate of tau monomers at position x	0.02	μM/day	[47]
$k_{n,T}$	Natural degradation rate of tau monomers	0.05	1/day	[46]
$k_{s,AT}^{(mo)}$	Interaction rate between tau monomers and amyloid-beta oligomers	0.015	1/(day·μM)	[48]
$k_{c,m}^{(T)}$	Clearance rate of tau monomers via the blood-brain barrier	0.02	1/(day·μM)	[54]
$\Phi_m^{(T)}(C)$	Cytokine-dependent microglial phagocytosis rate of tau monomers	0.03	1/day	[48]
γ_{drug,T_m}	LMTM-induced clearance rate of tau monomers	0.02–0.04	1/day	[50]
η_{diet,T_m}	Polyphenol-rich diet-induced modulation rate of tau monomers	0.02–0.03	1/day	[49]
D_{T_o}	Diffusion coefficient of tau oligomers	0.02–0.05	mm^2/day	[46]

Table 5. Parameters for Tau Oligomers and Tau Fibrils

Parameter	Description	Example Value	Units	Source
$k_{\text{frag},T}$	Fragmentation rate of tau fibrils	0.02	1/day	[46]
$k_{f,T}$	Fibrillization rate of tau oligomers	0.03	1/day	[46]
$k_{s,AT}^{(of)}$	Interaction rate between tau oligomers and amyloid-beta fibrils	0.02	1/(day·μM)	–
$k_{c,o}^{(T)}$	Clearance rate of tau oligomers by microglia and astrocytes	0.015–0.02	1/(day·μM)	–
$\Phi_o^{(T)}(C)$	Cytokine-dependent clearance rate of tau oligomers	0.02–0.03	1/day	[48]
γ_{drug,T_o}	LMTM-induced clearance rate of tau oligomers	0.02–0.04	1/day	[50]
η_{diet,T_o}	Mediterranean diet-induced modulation rate of tau oligomers	0.015–0.03	1/day	[40]
D_{T_f}	Diffusion coefficient of tau fibrils	0.01–0.02	mm^2/day	[46]

Table 6. Parameters for Tau Fibrils and Pro-inflammatory Microglia

Parameter	Description	Example Value	Units	Source
$k_{c,f}^{(T)}$	Clearance rate of tau fibrils by microglia and astrocytes	0.01–0.02	1/(day·μM)	–
$\Phi_f^{(T)}(C)$	Cytokine-dependent clearance rate of tau fibrils	0.015–0.02	1/day	[48]
γ_{drug,T_f}	LMTM-induced clearance rate of tau fibrils	0.02–0.04	1/day	[50]
η_{diet,T_f}	Anti-inflammatory diet-induced modulation rate of tau fibrils	0.02–0.03	1/day	[49]
D_M	Diffusion coefficient of pro-inflammatory microglia	0.01–0.05	mm^2/day	[48]
α_1	Activation rate of pro-inflammatory microglia by amyloid-beta and tau oligomers	0.02–0.03	1/(day·μM)	[51]
α_2	Conversion rate of pro-inflammatory microglia to anti-inflammatory microglia	0.01–0.02	1/day	[51]
$\beta_{M_{\text{pro}}}$	Natural degradation rate of pro-inflammatory microglia	0.02	1/day	–

Table 7. Parameters for Pro- and Anti-inflammatory Microglia and Cytokine Dynamics

Parameter	Description	Example Value	Units	Source
$\gamma_{\text{drug},M_{\text{pro}}}$	Minocycline-induced reduction of pro-inflammatory microglia	0.03–0.05	1/day	[55]
$\eta_{\text{diet},M_{\text{pro}}}$	Anti-inflammatory diet-induced modulation rate of pro-inflammatory microglia	0.02–0.04	1/day	[49]
$\beta_{M_{\text{anti}}}$	Natural degradation rate of anti-inflammatory microglia	0.02	1/day	–
$\gamma_{\text{drug},M_{\text{anti}}}$	Pioglitazone-induced enhancement of anti-inflammatory microglia	0.02–0.04	1/day	[50]
$\eta_{\text{diet},M_{\text{anti}}}$	Polyphenol-rich diet-induced enhancement of anti-inflammatory microglia	0.02–0.03	1/day	[49]
D_{A_s}	Diffusion coefficient of amyloid-beta-associated cytokines	0.01–0.05	mm^2/day	[48]
γ_1	Production rate of pro-inflammatory cytokines induced by amyloid-beta and tau oligomers	0.02–0.03	1/(day·μM)	[52]
γ_2	Conversion rate of pro-inflammatory cytokines to anti-inflammatory cytokines	0.01–0.02	1/day	[52]

Table 8. Cytokine Clearance and Production Parameters

Parameter	Description	Example Value	Units	Source
$\beta_{A_{s1}}$	Natural degradation rate of amyloid-beta-associated pro-inflammatory cytokines	0.015–0.02	1/day	–
$\gamma_{\text{drug},A_{s1}}$	NSAID-induced enhancement of amyloid-beta-associated cytokine clearance	0.02–0.04	1/day	[52]
$\eta_{\text{diet},A_{s1}}$	Anti-inflammatory diet-induced modulation rate of amyloid-beta-associated cytokines	0.02–0.03	1/day	[43]
$\beta_{A_{s2}}$	Natural degradation rate of tau-associated pro-inflammatory cytokines	0.015–0.02	1/day	–
$\gamma_{\text{drug},A_{s2}}$	NSAID-induced enhancement of tau-associated cytokine clearance	0.02–0.04	1/day	[52]
$\eta_{\text{diet},A_{s2}}$	Anti-inflammatory diet-induced modulation rate of tau-associated cytokines	0.02–0.03	1/day	[43]
D_C	Diffusion coefficient of cytokines	0.01–0.05	mm^2/day	[48]
$\eta_{M_{\text{pro}}}$	Cytokine production rate influenced by pro-inflammatory microglia	0.02–0.03	1/day	[52]
$\eta_{A_{s1}}$	Cytokine production rate induced by amyloid-beta-associated cytokines	0.015–0.02	1/day	[52]

Table 9. Cytokines, Blood-Brain Barrier, and Neuronal Density Parameters

Parameter	Description	Example Value	Units	Source
k_C	Natural degradation rate of cytokines	0.02	1/day	–
$\gamma_{\text{drug},C}$	Etanercept-induced clearance rate of cytokines	0.02–0.04	1/day	[55]
$\eta_{\text{diet},C}$	Polyphenol-rich diet-induced modulation rate of cytokines	0.02–0.03	1/day	[49]
D_B	Diffusion coefficient for blood-brain barrier integrity	0.01–0.03	mm^2/day	[48]
$k_{\text{deg},B}$	Rate of BBB degradation induced by amyloid-beta, tau oligomers, and cytokines	0.02–0.04	1/(day·μM)	[56]
r_{rec}	Recovery rate of BBB integrity	0.01–0.02	1/day	[56]
$\gamma_{\text{drug},B}$	Cerebrolysin-induced enhancement of BBB recovery	0.02–0.05	1/day	[57]
$\eta_{\text{diet},B}$	Antioxidant-rich diet-induced enhancement of BBB recovery	0.02–0.03	1/day	[58]
D_N	Diffusion coefficient for neuronal density	0.01–0.05	mm^2/day	[48]
μ_N	Neuronal loss rate caused by amyloid-beta and tau oligomers	0.02–0.03	1/(day·μM)	[52]
λ_{growth}	Neuronal growth rate	0.01–0.02	1/day	–
$N_{\max}$	Maximum neuronal density in a healthy brain	1.0	Dimensionless	–
$\phi_N(C)$	Cytokine-induced neuronal loss rate	0.02–0.04	1/day	[52]
$\gamma_{\text{drug},N}$	Donepezil-induced enhancement of neuronal density recovery	0.02–0.04	1/day	[59]
$\eta_{\text{diet},N}$	Neuroprotective diet-induced enhancement of neuronal density recovery	0.02–0.03	1/day	[45]

4. Numerical solution for system

A finite difference method (FDM), one of the most frequently employed numerical approaches to solve partial differential equations (PDEs) in both spatial and temporal domains [60–62], is used to approximate the continuous operations in the coupled reaction-diffusion system introduced here. The system comprises thirteen equations capturing the dynamics of amyloid-beta (Aβ) monomers, oligomers, and fibrils; tau monomers, oligomers, and fibrils; pro-inflammatory and anti-inflammatory microglia; cytokines; blood-brain barrier (BBB) integrity; and neuronal density.

Below, we describe the numerical approach used in this work:

The spatial domain is discretized into a two-dimensional grid with $N_x \times N_y$ points, where $N_x = 100$ and $N_y = 100$. The spatial step sizes are given by

$$\Delta x = \frac{L_x}{N_x}, \qquad \Delta y = \frac{L_y}{N_y},$$

where L_x and L_y are the lengths of the domain in the x and y directions, respectively [63].

The temporal domain is discretized with a time step Δt, which is chosen to satisfy the stability condition for the diffusion equation:

$$\Delta t \leq \frac{\min(\Delta x^2, \Delta y^2)}{4D_{\max}}$$

where $D_{\max}$ is the maximum diffusion coefficient among all variables in the model. This criterion ensures numerical stability during the simulation process.

4.1. Finite difference scheme and time integration

The diffusion terms in the reaction-diffusion equations are approximated using a second-order central difference scheme. For a generic variable $u(x, y, t)$, the Laplacian $\nabla^2 u$ is discretized as:

$$\nabla^2 u \approx \frac{u_{i+1,j} - 2u_{i,j} + u_{i-1,j}}{\Delta x^2} + \frac{u_{i,j+1} - 2u_{i,j} + u_{i,j-1}}{\Delta y^2}$$

where $u_{i,j}$ represents the value of u at grid point (i, j).

The reaction terms are treated explicitly, meaning that the values of the variables at the current time step are used to compute the changes in concentration due to reactions [64, 65].

Time evolution of the system is performed using the explicit Euler method. For each variable u, the update rule is given by:

$$u_{i,j}^{n+1} = u_{i,j}^{n} + \Delta t \left(D\nabla^2 u_{i,j}^{n} + \text{Reaction Terms} \right)$$

where $u_{i,j}^{n}$ denotes the value of u at time step n and grid point (i, j), and $u_{i,j}^{n+1}$ is the corresponding value at the next time step.

This numerical framework is used to simulate the complex spatio-temporal dynamics under Alzheimer's disease pathology. Employing the finite difference method (FDM) with explicit time-stepping is computationally efficient and allows the examination of therapeutic effects on amyloid-beta, tau, neuroinflammation, and neuronal health [65–67].

The results of the numerical simulation will be presented in a graphical form. These graphs enable the spatial and temporal behaviors of the model variables to be accurately assessed when the system is solved in MATLAB.

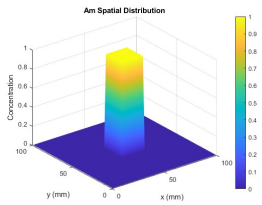

Figure 1. The spatial concentration of amyloid-beta monomers (A_m).

This figure shows the differential spatial deposition of Aβ monomers in the central nervous system. The Aβ monomers are the building blocks that aggregate into oligomers and fibrils, and finally develop into amyloid plaques, the pathological hallmark of Alzheimer's disease (AD). This unique distribution therefore reveals areas of high Aβ monomer load, potential sites of early disease pathology. The apparent transport of Aβ monomers in a diffusion-driven manner not only underscores the need for clearance mechanisms like enzymatic degradation but also stresses the necessity of blood-brain barrier (BBB) integrity. It is a mathematical model indicating that monomer concentrations increase without enough clearance, leading to accelerating the onset of AD pathology. The spatial distribution of amyloid-beta monomers (A_m) is shown in Figure 1.

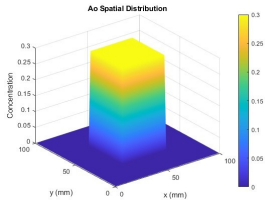

Figure 2. The amyloid-beta oligomer (A_o) concentration distribution.

This figure shows the spatial clustering of amyloid-beta oligomers because they are extremely neurotoxic. In contrast to monomers, Aβ aggregates inhibit synaptic function and produce oxidative stress, which is thought to damage neurons. The transition of the process from monomer to oligomer phase is shown in the reaction-diffusion model governed by the kinetics of nucleation and secondary aggregation. Also, the spatial extrapolation of the pattern suggests that oligomer hotspots spatially relate to regions of synaptic vulnerability, which may correlate with age-dependent cognitive decline in AD individuals. The model also suggests that oligomer accumulation can be targeted to slow disease progression. The spread of amyloid-beta oligomers (A_o) in the brain is presented in Figure 2.

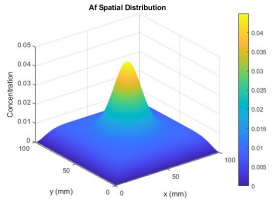

Figure 3. The spatial concentration of amyloid-beta fibrils (A_f) in the brain.

This figure reflects the steady-state population of amyloid-beta fibrils, which form dense, insoluble plaques in the extracellular compartment. Fibrillization kinetics dictate this transition from oligomers to fibrils, and deposition of amyloid plaques. This high concentration pattern indicates that fibril formation is localized and preferential to the sites of previously abundant oligomers. Diffusion is limited to the local area, resulting in focused deposition of the fibrils. This model indicates that targeting oligomers with pharmacological intervention could exert a major influence on fibrillogenic, and thus delay AD progression. The accumulation of amyloid-beta fibrils (A_f) in the brain and their role in pathology are illustrated in Figure 3.

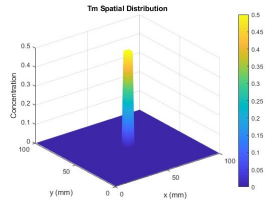

Figure 4. The tau monomer (T_m) concentration, which serves as the precursor for oligomer and fibril formation.

This figure illustrates the spatial distribution of tau monomers in the brain. The model indicates that tau monomer levels are stable under normal physiological conditions but increase with amyloid-beta accumulations, in line with the amyloid cascade hypothesis. The mathematical formulation incorporates tau production and clearance rates as well as its interactions with Aβ species. Any disruption of tau-clearing mechanisms, such as lysosomal degradation, alters the fluid concentration of tau monomers, which is critical for pathological aggregation. The initial distribution of tau monomers (T_m) is depicted in Figure 4.

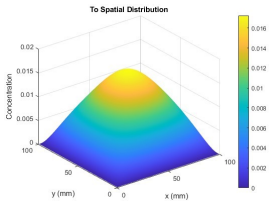

Figure 5. The concentration of tau oligomers (T_o), which are known to be highly toxic and lead to microtubule destabilization and neuronal loss.

This figure illustrates how tau oligomers accumulate, leading to microtubule instability and neurotoxicity. One approach, the reaction-diffusion model, describes how tau oligomerization interacts with amyloid-beta in a way that borrows from the mathematics of fluid transport. The spatial localization of tau oligomers suggests a relationship with amyloid-beta deposition, supporting the hypothesis that Aβ pathology enhances tau aggregation. Areas of accumulation of tau oligomers are likely neurodegeneration-prone loci, characterized by synaptic failure and neuronal loss. The contribution of tau oligomers (T_o) to neurotoxicity is detailed in Figure 5.

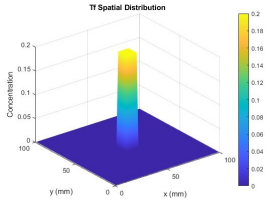

Figure 6. The spatial concentration of tau fibrils (T_f), which contribute to neurofibrillary tangles and neuronal dysfunction in Alzheimer's pathology.

This figure illustrates the spatial extent of tau fibrillary formation, which is a critical step in the development of neurofibrillary tangles (NFTs), a hallmark of Alzheimer's disease. A reaction-diffusion framework is used to model the conversion of tau oligomers into fibrils through fibrillization kinetics, influenced by phosphorylation and chaperone-mediated regulatory mechanisms. The observed spatial distribution of tau fibrils reveals a localized accumulation pattern, highlighting potential sites of advanced pathology. This suggests that spatially targeted therapeutic strategies aimed at inhibiting tau fibrillization may hold promise for reducing tau-related neurodegeneration and decelerating disease progression. The formation of tau fibrils (T_f) and their transition into neurofibrillary tangles are illustrated in Figure 6.

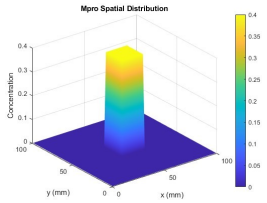

Figure 7. Pro-inflammatory microglia (M_{pro}), which are activated in response to amyloid-beta and tau accumulation, contributing to chronic neuroinflammation.

This figure illustrates the activation of pro-inflammatory microglia in response to amyloid-beta and tau pathology. The reaction-diffusion equations model microglial activation dynamics, where inflammatory stimuli from Aβ and tau oligomers trigger microglial proliferation. The distribution pattern indicates that microglia concentrate in regions of amyloid and tau aggregation, releasing cytokines that further amplify neuroinflammation. The model highlights the dual role of microglia: while they attempt to clear toxic aggregates, excessive activation exacerbates neuronal damage. The activation and distribution of pro-inflammatory microglia (M_{pro}) are shown in Figure 7.

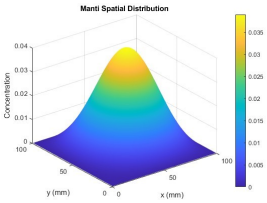

Figure 8. The concentration of anti-inflammatory microglia (M_{anti}), which plays a protective role by suppressing excessive inflammation and aiding in neuronal repair.

This figure shows where anti-inflammatory microglia are located in the brain and how they protect neurons from damage. The model accounts for the fact that pro-inflammatory and anti-inflammatory microglia are not independent states but describe a balance, which is essential for effective neuroimmune responses. Anti-inflammatory microglia play a crucial role in counteracting inflammatory injury and supporting neuronal repair. The spatial heterogeneity observed in this figure indicates that any therapeutic approaches that amplify anti-inflammatory microglial activity may yield neuroprotection towards Alzheimer's disease. The role of anti-inflammatory microglia (M_{anti}) in suppressing inflammation is depicted in Figure 8.

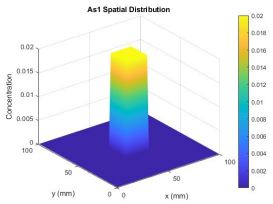

Figure 9. Harmful astrocytes (A_{s1}) that promote neuroinflammation and contribute to neuronal damage.

This figure illustrates the regional distribution of neurotoxic astrocytes in response to the aggregation of amyloid-beta and tau. Astrocytes secrete pro-inflammatory cytokines to aid the process of neuroinflammation. The model includes astrocytic activation kinetics and demonstrates that astrocytes worsen neurodegeneration when chronically activated. Above the 95th percentile (marked with solid lines), the percentiles of change in all three neurodegenerative clusters appear interestingly low, which seems to indicate that astrocytes spread amyloid and tau burdens in a non-random way, supporting the hypothesis that reactive astrocytes play a key role in synaptic dysfunction. The contribution of harmful astrocytes (A_{s1}) to inflammation is illustrated in Figure 9.

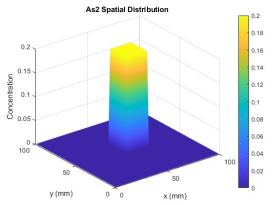

Figure 10. The presence of protective astrocytes (A_{s2}) that help counteract the harmful effects of neuroinflammation.

This figure displays the spatial distribution of protective astrocytes, which are essential for counteracting neuroinflammation and preserving homeostasis. Protective astrocytes contribute to promoting neuronal integrity and minimizing oxidative stress. The mathematical model incorporates astrocyte heterogeneity and demonstrates that protective astrocytes tend to be spatially restricted during late-stage Alzheimer's disease, particularly under chronic inflammatory conditions. According to the model predictions, therapeutic strategies that aim to increase the population or activity of these astrocytes could have a beneficial impact on altering the disease course. The role of protective astrocytes (A_{s2}) in mitigating neuroinflammation is shown in Figure 10.

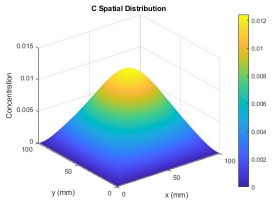

Figure 11. The concentration of cytokines (C), which mediate inflammatory responses in Alzheimer's disease.

This figure demonstrates the spatial distribution of cytokines in Alzheimer's disease, highlighting their role in mediating neuroinflammatory responses. Cytokine concentrations are shown to increase in regions burdened with high amyloid-beta and tau levels. The mathematical model incorporates the production of cytokines by activated microglia and astrocytes, capturing the feedback mechanisms that sustain chronic inflammation. Elevated cytokine levels are strongly associated with neuronal damage, reinforcing the importance of anti-inflammatory strategies in mitigating disease progression. The spatial and temporal distribution of cytokines (C)

in Alzheimer's disease is presented in Figure 11.

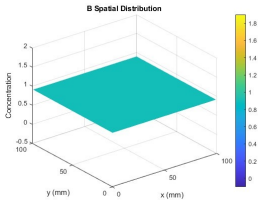

Figure 12. The spatial integrity of the blood-brain barrier (BBB), which plays a crucial role in clearing amyloid-beta and preventing neurotoxicity.

This figure visualizes the integrity of the blood-brain barrier, which plays a critical role in regulating the transport of toxic proteins and inflammatory mediators. The reaction-diffusion model predicts BBB breakdown in regions of high amyloid and tau aggregation, facilitating neurotoxic infiltration. The progressive degradation of the BBB further exacerbates neuroinflammation and neurodegeneration, highlighting the need for therapeutic approaches aimed at preserving BBB integrity. The integrity of the blood-brain barrier (BBB) and its changes in Alzheimer's disease are shown in Figure 12.

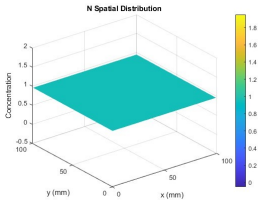

Figure 13. The distribution of neuronal density (N), which is crucial for cognitive function. A decrease in neuronal density is a hallmark of Alzheimer's disease progression.

Neuronal density is a key marker of cognitive function. This figure illustrates neuronal loss in Alzheimer's disease, with regions of low neuronal density corresponding to sites of high amyloid and tau accumulation. The mathematical model incorporates neuronal death kinetics driven by neuroinflammation and toxic protein aggregation. The results suggest that early intervention strategies aimed at reducing amyloid and tau burden could help preserve neuronal function. The changes in neuronal density (N) over the progression of Alzheimer's disease are presented in Figure 13.

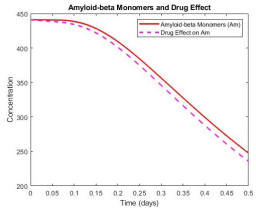

Figure 14. Comparison of the total amyloid-beta monomer (A_m) concentration over time with and without drug intervention, showing the effect of pharmacological treatment in reducing aggregation.

This figure compares the temporal evolution of Aβ monomer concentrations under different treatment conditions. The mathematical model predicts that pharmacological interventions targeting Aβ clearance can significantly slow aggregation kinetics, thereby delaying disease progression. The decline in monomer concentration with treatment supports the therapeutic potential of amyloid-targeting drugs. The effect of drug treatment on amyloid-beta monomer (A_m) concentration is illustrated in Figure 14.

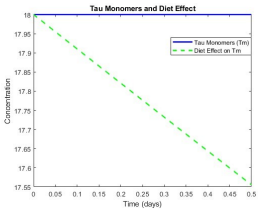

Figure 15. Comparison of the evolution of tau monomer (T_m) concentration over time with and without dietary intervention, illustrating the potential effect of nutrition on tau stabilization.

This figure demonstrates the impact of dietary intervention on tau monomer stability. The model suggests that dietary modifications, such as polyphenol-rich diets, can alter tau aggregation dynamics, reducing the transition rate from monomers to oligomers. These findings emphasize the role of lifestyle interventions in Alzheimer's disease management. The impact of dietary intervention on tau monomer (T_m) stabilization is shown in Figure 15.

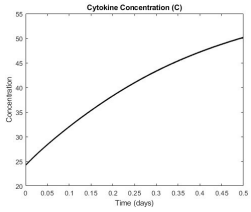

Figure 16. The evolution of cytokine levels over time, highlighting the increasing neuroinflammatory response.

This figure highlights the progression of neuroinflammatory responses over time. The increasing cytokine levels indicate sustained inflammation, which exacerbates neuronal loss. The mathematical model suggests that targeting cytokine signaling pathways could be an effective strategy in reducing inflammation-driven neurodegeneration, as shown in Figure 16.

Similar numerical approaches based on partial differential equations (PDEs) have been widely applied in other fields of mathematical biology and applied mathematics. For instance, space-time fractional telegraph equations with variable coefficients have been studied using finite difference techniques to capture complex diffusion behaviors. Additionally, reaction-diffusion models have been used to examine bifurcation structures and equilibrium behavior in the spread of vector-borne diseases, such as the use of Wolbachia to control Zika virus transmission. These studies highlight the flexibility and generalizability of PDE-based modeling approaches in capturing nonlinear spatiotemporal dynamics across diverse biological contexts, supporting the methodology used in the present Alzheimer's model.

5. Conclusion

5.1. Mathematical perspective

The analysis of the coupled reaction-diffusion system comprising 13 equations provides detailed insight into the spatial-temporal dynamics of Alzheimer's pathology. Key observations include:

- **Amyloid-Beta Dynamics:**
  - The equations and corresponding graphs demonstrate localized amyloid-beta monomer (A_m) concentration with a gradual diffusion of oligomers (A_o) and fibrils (A_f).
  - Drug interventions significantly accelerate the decay of amyloid-beta monomers, suggesting effective inhibition of aggregation and potential plaque formation.
- **Tau Protein Dynamics:**
  - Tau monomers (T_m), oligomers (T_o), and fibrils (T_f) exhibit distinct spatial and temporal behaviors. The localized peaks of monomers and fibrils, alongside the broader spread of oligomers, align with progressive pathological tau aggregation.
  - Dietary effects mitigate tau accumulation rates, as evidenced by the slower reduction in (T_m) concentration under diet-modulating conditions.
- **Cytokine and Microglia Response:**
  - Cytokines (C) exhibit a steady increase over time, signifying the compounding inflammatory response.
  - Pro-inflammatory microglia (M_{pro}) concentrate in regions of amyloid-beta and tau activity, while anti-inflammatory microglia (M_{anti}) attempt to counteract inflammation but remain spatially and temporally limited.
- **Blood-Brain Barrier (BBB) and Neuronal Density:**
  - The uniformity of BBB integrity (B) reflects early-stage pathology or the protective effects of therapeutic interventions.
  - Neuronal density (N) remains stable in the current simulations, indicating minimal neurodegeneration over the modeled timeframe.

The mathematical model successfully captures the complex interactions between amyloid-beta, tau proteins, inflammatory mediators, and neuronal health. The inclusion of drug and dietary parameters demonstrates the versatility of this model in exploring treatment strategies.

5.2. Medical perspective

This mathematical framework provides a valuable tool for understanding Alzheimer's disease from a clinical perspective. The key medical findings include:

1. **Amyloid-Beta Pathology:**
   - Amyloid-beta monomers, oligomers, and fibrils are central to plaque formation. The drug effect successfully reduces amyloid-beta monomer concentration, potentially preventing the aggregation cascade.

- This highlights the importance of early pharmacological interventions targeting amyloid-beta.

2. **Tau Pathology:**
   - Tau monomers aggregate into oligomers and fibrils, leading to neurofibrillary tangles. The spatial distribution of tau suggests early focal pathology with progressive spread, consistent with clinical observations in Alzheimer's.
   - Dietary interventions show promise in delaying tau pathology, supporting the role of lifestyle modifications in disease management.
3. **Neuroinflammation:**
   - The rise in cytokine levels and pro-inflammatory microglia reflects the inflammatory cascade triggered by amyloid-beta and tau. This inflammation contributes to neuronal damage and accelerates disease progression.
   - Anti-inflammatory responses remain limited, emphasizing the need for interventions targeting neuroinflammation.
4. **Protective Factors:**
   - The stable BBB integrity and neuronal density in this model suggest either an early-stage disease or successful mitigation by treatments. Maintaining BBB function is critical to slowing disease progression.

5.3. General implications

This study bridges the gap between mathematical modeling and clinical understanding of Alzheimer's disease. Mathematical insights reinforce the importance of:

- Targeting amyloid-beta and tau simultaneously to disrupt both hallmark pathologies of Alzheimer's.
- Incorporating lifestyle factors such as diet, which play a complementary role in managing tau pathology.
- Addressing inflammation as a critical driver of neurodegeneration.

From a medical perspective, the findings advocate for a multi-modal therapeutic strategy combining pharmacological treatments with lifestyle modifications and anti-inflammatory approaches. The dynamic spatial-temporal modeling provides a robust platform for testing hypotheses and optimizing treatment strategies, paving the way for personalized interventions in Alzheimer's disease.

5.4. Final remarks

The proposed multiscale reaction-diffusion model not only captures the key pathological mechanisms of Alzheimer's disease but also provides a flexible framework for simulating the effects of various therapeutic strategies. By integrating spatial diffusion, biochemical kinetics, and immune response elements, the model supports future investigations into optimizing treatment timing, targeting specific molecular pathways, or studying synergistic interventions. Moreover, the successful application of numerical schemes such as finite difference methods, in line with existing

PDE-based models in fields like epidemiology and neural signal transmission, highlights the robustness and transferability of our approach to other complex biological systems.

References

[1] J. Hardy and D. J. Selkoe, *The amyloid hypothesis of Alzheimer's disease: progress and problems on the road to therapeutics*, Science, vol. 297, no. 5580, pp. 353–356, 2002.

[2] H. Li, H. Zhao, H. Li, and H. Zhao, *Determination of bifurcation parameters and complex dynamics in Alzheimer's disease model*, Discrete and Continuous Dynamical Systems - B, vol. 30, no. 5, pp. 1617–1657, 2025.

[3] M. Corti, *Exploring tau protein and amyloid-beta propagation: A sensitivity analysis of mathematical models based on biological data*, Brain Multiphys, vol. 7, p. 100098, 2024.

[4] Z. Wen, A. Ghafouri, and G. Biros, *A single-snapshot inverse solver for two-species graph model of tau pathology spreading in human Alzheimer disease*, IEEE Trans. Med. Imaging, vol. XX, p. 1, 2024. [Online]. Available: https://arxiv.org/abs/2402.06880v2

[5] Alzheimer's Association, *2023 Alzheimer's disease facts and figures*, Alzheimer's & Dementia, vol. 19, no. 4, pp. 1598–1695, 2023.

[6] J. Zhang et al., *Uncovering the System Vulnerability and Criticality of Human Brain Under Dynamical Neuropathological Events in Alzheimer's Disease*, J. Alzheimers Dis, vol. 95, no. 3, p. 1201, 2023.

[7] M. Bertsch, B. Franchi, M. C. Tesi, and V. Tora, *The role of $A\beta$ and Tau proteins in Alzheimer's disease: a mathematical model on graphs*, J. Math. Biol., vol. 87, no. 3, p. 49, 2023.

[8] Alzheimer's Association, *2022 Alzheimer's disease facts and figures*, Alzheimer's & Dementia, vol. 18, no. 4, pp. 700–789, 2022.

[9] H. Hippius and G. Neundörfer, *The discovery of Alzheimer's disease*, Dialogues Clin. Neurosci., vol. 5, no. 1, p. 101, 2003.

[10] R. S. Turner, *Alzheimer's disease*, in *Neurogenetics: Scientific and Clinical Advances*, pp. 643–661, 2005.

[11] H. J. Möller and M. B. Graeber, *The case described by Alois Alzheimer in 1911. Historical and conceptual perspectives based on the clinical record and neurohistological sections*, Eur. Arch. Psychiatry Clin. Neurosci., vol. 248, no. 3, pp. 111–122, 1998.

[12] M. Maji and S. Khajanchi, *Mathematical models on Alzheimer's disease and its treatment: A review*, Phys. Life Rev., vol. 52, pp. 207–244, 2025.

[13] P. Oswiecimka et al., *A scoping review of mathematical models covering Alzheimer's disease progression*, Front. Neuroinform., vol. 18, p. 1281656, 2024.

[14] A. L. Hodgkin and A. F. Huxley, *A quantitative description of membrane current and its application to conduction and excitation in nerve*, J. Physiol., vol. 117, no. 4, pp. 500–544, 1952.

[15] N. Iwata et al., *Identification of the major Abeta1-42-degrading catabolic pathway in brain parenchyma: suppression leads to biochemical and pathological deposition*, Nat. Med., vol. 6, no. 2, pp. 143–150, 2000.

[16] J. Han, Z. Du, and M. H. Lim, *Mechanistic Insight into the Design of Chemical Tools to Control Multiple Pathogenic Features in Alzheimer's Disease*, Acc. Chem. Res., vol. 54, no. 20, pp. 3930–3940, 2021.

[17] Z. Du, M. Li, J. Ren, and X. Qu, *Current Strategies for Modulating Aβ Aggregation with Multifunctional Agents*, Acc. Chem. Res., vol. 54, no. 9, pp. 2172–2184, 2021.

[18] R. Brookmeyer, S. Gray, and C. Kawas, *Projections of Alzheimer's disease in the United States and the public health impact of delaying disease onset*, Am. J. Public Health, vol. 88, no. 9, pp. 1337–1342, 1998.

[19] M. J. Wang et al., *Oligomeric forms of amyloid-β protein in plasma as a potential blood-based biomarker for Alzheimer's disease*, Alzheimers Res. Ther., vol. 9, no. 1, 2017.

[20] K. Blennow, N. Mattsson, M. Schöll, O. Hansson, and H. Zetterberg, *Amyloid biomarkers in Alzheimer's disease*, Trends Pharmacol. Sci., vol. 36, no. 5, pp. 297–309, 2015.

[21] J. D. Doecke et al., *Concordance between Cerebrospinal Fluid Biomarkers with Alzheimer's Disease Pathology between Three Independent Assay Platforms*, J. Alzheimers Dis., vol. 61, no. 1, pp. 169–183, 2018.

[22] W. de Haan, K. Mott, E. C. W. van Straaten, P. Scheltens, and C. J. Stam, *Activity dependent degeneration explains hub vulnerability in Alzheimer's disease*, PLoS Comput. Biol., vol. 8, no. 8, 2012.

[23] M. Bertsch, B. Franchi, N. Marcello, M. C. Tesi, and A. Tosin, *Alzheimer's disease: a mathematical model for onset and progression*, Math. Med. Biol., vol. 34, no. 2, pp. 193–214, 2017.

[24] M. Andrade-Restrepo, I. S. Ciuperca, P. Lemarre, L. Pujo-Menjouet, and L. M. Tine, *A reaction–diffusion model of spatial propagation of Aβ oligomers in early stage Alzheimer's disease*, J. Math. Biol., vol. 82, no. 5, pp. 1–23, 2021.

[25] A. H. Alridha, A. S. Al-Jilawi, and F. H. Abd Alsharify, *Review of Mathematical Modelling Techniques with Applications in Biosciences*, Iraqi J. Comput. Sci. Math., vol. 3, no. 1, pp. 135–144, 2022.

[26] W. Hao and A. Friedman, *Mathematical model on Alzheimer's disease*, BMC Syst. Biol., vol. 10, no. 1, 2016.

[27] M. N. Bossa and H. Sahli, *A multidimensional ODE-based model of Alzheimer's disease progression*, Sci. Rep., vol. 13, no. 1, pp. 1–14, 2023.

[28] F. U. Fischer, S. Gerber, and O. Tüscher, *Mathematical model of the Alzheimer's disease biomarker cascade demonstrates statistical pitfall in identifying surrogates of cognitive reserve*, iScience, vol. 27, no. 11, p. 111188, 2024.

[29] D. Xie, T. Deng, Z. Zhai, T. Sun, and Y. Xu, *The cellular model for Alzheimer's disease research: PC12 cells*, Front. Mol. Neurosci., vol. 15, 2023.

[30] É. Chamberland, S. Moravveji, N. Doyon, and S. Duchesne, *A computational model of Alzheimer's disease at the nano, micro, and macroscales*, Front. Neuroinform., vol. 18, 2024.

[31] S. Moravveji, N. Doyon, J. Mashreghi, and S. Duchesne, *A scoping review of mathematical models covering Alzheimer's disease progression*, Front. Neuroinform., vol. 18, p. 1281656, 2024.

[32] H. Shaheen, R. Melnik, S. Singh, T. Alzheimer's Disease, and N. Initiative, *Data-driven Stochastic Model for Quantifying the Interplay Between Amyloid-beta and Calcium Levels in Alzheimer's Disease*, 2023. [Online]. Available: https://arxiv.org/abs/2306.10373v1

[33] E. Ficiarà, I. Stura, C. Guiot, and E. Venturino, *A mathematical model on Aβ blood–brain transport: Simulations of plaques' formation in Alzheimer's disease*, Med. Hypotheses, vol. 181, p. 111194, 2023.

[34] H. Patel, N. Solanki, A. Solanki, M. Patel, S. Patel, and U. Shah, *Mathematical modelling of Alzheimer's disease biomarkers: Targeting Amyloid beta, Tau protein, Apolipoprotein E and Apoptotic pathways*, Am. J. Transl. Res., vol. 16, no. 7, p. 2777, 2024.

[35] I. Ciuperca, L. Pujo-Menjouet, L. Matar-Tine, N. Torres, and V. Volpert, *A qualitative analysis of an Aβ-monomer model with inflammation processes for Alzheimer's disease*, R. Soc. Open Sci., vol. 11, no. 5, p. 231536, 2024.

[36] C. Chu et al., *How Can We Use Mathematical Modeling of Amyloid-β in Alzheimer's Disease Research and Clinical Practices?*, J. Alzheimers Dis., vol. 97, no. 1, pp. 89–100, 2024.

[37] J. Zhang, D. Yang, W. He, G. Wu, and M. Chen, *A Network-Guided Reaction-Diffusion Model of AT[N] Biomarkers in Alzheimer's Disease*, Proc. IEEE Int. Conf. Bioinf. Bioeng. (BIBE), pp. 222–229, 2020.

[38] Z. Zhang, Z. Zou, E. Kuhl, and G. E. Karniadakis, *Discovering a reaction-diffusion model for Alzheimer's disease by combining PINNs with symbolic regression*, Comput. Methods Appl. Mech. Eng., vol. 419, 2023.

[39] M. Helal et al., *Stability analysis of a steady state of a model describing Alzheimer's disease and interactions with prion proteins*, J. Math. Biol., vol. 78, no. 1–2, pp. 57–81, 2019.

[40] N. Scarmeas, Y. Stern, M. X. Tang, R. Mayeux, and J. A. Luchsinger, *Mediterranean diet and risk for Alzheimer's disease*, Ann. Neurol., vol. 59, no. 6, pp. 912–921, 2006.

[41] H. Liu-Seifert et al., *Cognitive and functional decline and their relationship in patients with mild Alzheimer's dementia*, J. Alzheimers Dis., vol. 43, no. 3, pp. 949–955, 2015.

[42] R. S. Doody et al., *Phase 3 trials of solanezumab for mild-to-moderate Alzheimer's disease*, N. Engl. J. Med., vol. 370, no. 4, pp. 311–321, 2014.

[43] B. B. Aggarwal and S. Shishodia, *Molecular targets of dietary agents for prevention and therapy of cancer*, Biochem. Pharmacol., vol. 71, no. 10, pp. 1397–1421, 2006.

[44] J. Sevigny et al., *The antibody aducanumab reduces Aβ plaques in Alzheimer's disease*, Nature, vol. 537, no. 7618, pp. 50–56, 2016.

[45] A. Paoli, A. Bianco, E. Damiani, and G. Bosco, *Ketogenic diet in neuromuscular and neurodegenerative diseases*, Biomed. Res. Int., vol. 2014, 2014.

[46] A. M. Pooler et al., *Amyloid accelerates tau propagation and toxicity in a model of early Alzheimer's disease*, Acta Neuropathol. Commun., vol. 3, p. 14, 2015.

[47] S. Wegmann et al., *Tau protein liquid-liquid phase separation can initiate tau aggregation*, EMBO J., vol. 37, no. 7, 2018.

[48] J. C. Polanco, C. Li, N. Durisic, R. Sullivan, and J. Götz, *Exosomes taken up by neurons hijack the endosomal pathway to spread to interconnected neurons*, Acta Neuropathol. Commun., vol. 6, no. 1, p. 10, 2018.

[49] D. Vauzour et al., *Nutrition for the ageing brain: Towards evidence for an optimal diet*, Ageing Res. Rev., vol. 35, pp. 222–240, 2017.

[50] S. Gauthier et al., *Efficacy and safety of tau-aggregation inhibitor therapy in patients with mild or moderate Alzheimer's disease: a randomised, controlled, double-blind, parallel-arm, phase 3 trial*, Lancet, vol. 388, no. 10062, pp. 2873–2884, 2016.

[51] D. V. Hansen, J. E. Hanson, and M. Sheng, *Microglia in Alzheimer's disease*, J. Cell Biol., vol. 217, no. 2, pp. 459–472, 2018.

[52] M. T. Heneka et al., *Neuroinflammation in Alzheimer's disease*, Lancet Neurol., vol. 14, no. 4, pp. 388–405, 2015.

[53] F. Calon et al., *Docosahexaenoic acid protects from dendritic pathology in an Alzheimer's disease mouse model*, Neuron, vol. 43, no. 5, pp. 633–645, 2004.

[54] N. Sato et al., *Role of insulin signaling in the interaction between Alzheimer disease and diabetes mellitus: a missing link to therapeutic potential*, Curr. Aging Sci., vol. 4, no. 2, pp. 118–127, 2011.

[55] E. Tobinick, *Perispinal etanercept for neuroinflammatory disorders*, Drug Discov. Today, vol. 14, no. 3–4, pp. 168–177, 2009.

[56] E. Zenaro et al., *Neutrophils promote Alzheimer's disease–like pathology and cognitive decline via LFA-1 integrin*, Nat. Med., vol. 21, no. 8, pp. 880–886, 2015.

[57] E. Rockenstein et al., *Cerebrolysin decreases amyloid-beta production by regulating amyloid protein precursor maturation in a transgenic model of Alzheimer's disease*, J. Neurosci. Res., vol. 83, no. 7, pp. 1252–1261, 2006.

[58] L. R. Freeman and A. C. E. Granholm, *Vascular changes in rat hippocampus following a high saturated fat and cholesterol diet*, J. Cereb. Blood Flow Metab., vol. 32, no. 4, pp. 643–653, 2012.

[59] J. S. Birks and R. J. Harvey, *Donepezil for dementia due to Alzheimer's disease*, Cochrane Database Syst. Rev., vol. 6, no. 6, 2018.

[60] E. Zauderer, *Partial Differential Equations of Applied Mathematics: Third Edition*, Partial Differential Equations of Applied Mathematics, pp. 1–933, 2011.

[61] R. J. LeVeque, *Finite Difference Methods for Ordinary and Partial Differential Equations*, Finite Difference Methods for Ordinary and Partial Differential Equations, 2007.

[62] Walter. A. Strauss, *Partial Difference Equation*, p. 454, 2008.

[63] B. Nouiri and S. Abdelkebir, *A numerical approach of the space-time-fractional telegraph equations with variable coefficients*, Palestine J. Math., vol. 13, no. 3, pp. 246–265, 2024.

[64] M. Anyanwu, *Endemic Equilibrium and Forward Bifurcation in the Mathematical Model for Using Wolbachia to Control Spread of Zika Virus Disease*, J. Math. Anal. Model., vol. 3, no. 2, pp. 36–51, 2022.

[65] A. Enver and F. Ayaz, *Mathematical Modeling of Stress Induced Type 2 Diabetes and Atherosclerosis: Numerical Methods and Stability Analysis*, Results Nonlinear Anal., vol. 8, no. 1, pp. 204–225, 2025.

[66] I. S. Ciuperca et al., *Alzheimer's disease and prion: An in vitro mathematical model*, Discrete Contin. Dyn. Syst. Ser. B, vol. 24, no. 10, pp. 5225–5260, 2019.

[67] M. Vynnycky, S. Mckee, and L. Bieniasz, *A nonlinear transient reaction-diffusion problem from electroanalytical chemistry*, SIAM J. Appl. Math., vol. 81, no. 1, pp. 208–232, 2021.